**Supplementary Information**

# Acute loss of iron–sulfur clusters results in metabolic reprogramming and generation of lipid droplets in mammalian cells

**Daniel R. Crooks[1], Nunziata Maio[2], Andrew N. Lane[3], Michal Jarnik[4], Richard M. Higashi[3], Ronald G. Haller[5], Ye Yang[1], T. W-M. Fan[3], W. Marston Linehan[1], Tracey A. Rouault[2]**

From the [1]Urologic Oncology Branch, Center for Cancer Research, National Cancer Institute, Bethesda, MD 20892; [2]Section on Human Iron Metabolism, *Eunice Kennedy Shriver* National Institute of Child Health and Human Development, Bethesda, MD 20892; [3]Center for Environmental and Systems Biochemistry, Department of Toxicology and Cancer Biology and Markey Cancer Center, University of Kentucky, Lexington, Kentucky 40536, USA; [4]Section on Cell Biology and Metabolism, *Eunice Kennedy Shriver* National Institute of Child Health and Human Development, National Institutes of Health, Bethesda, MD 20892, USA; [5]Department of Neurology, University of Texas Southwestern Medical Center and VA North Texas Medical Center, and Neuromuscular Center, Institute for Exercise and Environmental Medicine, Dallas, Texas 75231

| primer # | primer name | sequence | purpose |
|---|---|---|---|
| **DRC001** | hISCU forward | attaagcttccaccatggcggcggctggggctttc | For cloning ISCU2 with HindIII upstream site and kozak sequence |
| **DRC003** | hISCU reverse | cg*cctcgag* ctacagatcttcttcagaaataagtttttgttctttcttctctgcctctccttttttggg | universal hISCU reverse primer with myc tag and XhoI site |
| **DRC004** | emGFP forward | att*aagctt* ccaccatggtgagcaagggcgaggagctgttc | with HindIII site upstream and kozak sequence |
| **DRC005** | emGFP reverse | cgcctcgagctacagatcttcttcagaaataagtttttgttccttgtacagctcgtccatgccgag | with myc tag and XhoI site |
| **DRC048** | hISCU-D37A forward | ccagcatgtggtgccgtaatgaaatta | site-directed mutagenesis; 5' phosphorylated and HPLC purified. |
| **DRC049** | hISCU-D37A reverse | agcccccaccagtccagttccaacatt | site-directed mutagenesis; 5' phosphorylated and HPLC purified. |
| **DRC053** | hISCU-C35S forward | ccagcaagtggtgacgtaatgaaatta | site-directed mutagenesis; 5' phosphorylated and HPLC purified. |

**Table 1: PCR primer sequences used in this study**

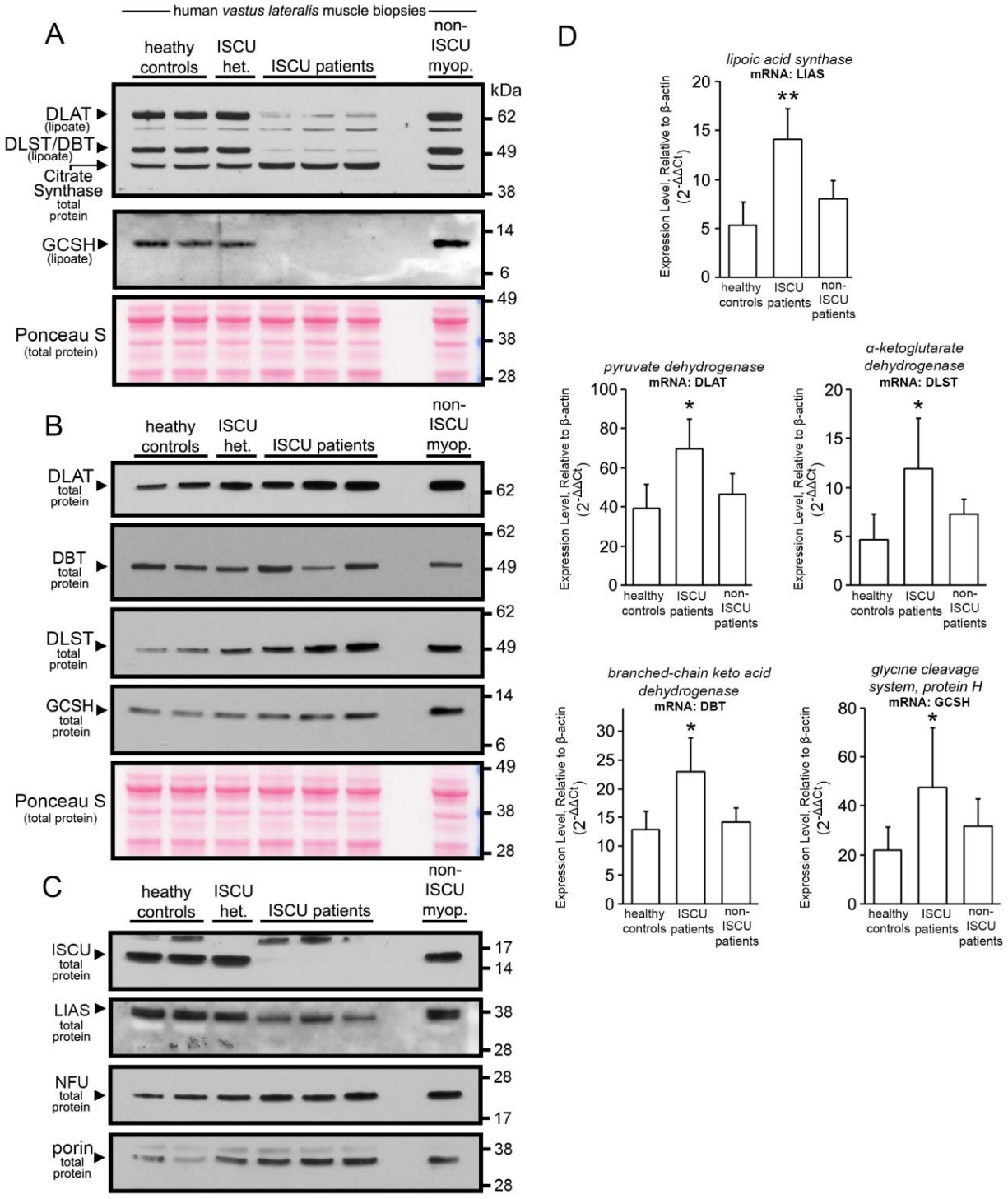


**Figure S1: Defective lipoylation of protein subunits in skeletal muscle biopsies from ISCU myopathy patients.** (A) Protein lipoylation in ISCU myopathy patient muscle biopsies was evaluated by immunoblot using an antibody specific to lipoylated lysine residues. The membrane was re-blotted with an antibody against citrate synthase to evaluate abundance of a non-lipoylated mitochondrial protein. Protein loading was assessed by Ponceau-S staining of total proteins on the membrane. (B) Immunoblots for total protein levels of lipoate-containing subunits revealed no decrease in subunit protein levels in the

patient samples. (C) Immunoblots confirmed strongly-decreased abundance of ISCU and LIAS protein level in patient muscle biopsies, whereas abundance of NFU and porin proteins was not decreased. Porin/VDAC1 immunoblot served as a loading control for mitochondrial protein. (D) qPCR was used to evaluate mRNA expression of LIAS and the LIAS targets DLAT, DLST, DBT and GCSH. T-tests were used to evaluate statistical differences between either the healthy controls (n=6) vs ISCU myopathy patients (n=3), or between healthy controls and non-ISCU myopathy patients (n=5). Data are mean±SD *$p<0.05$, **$p<0.01$.

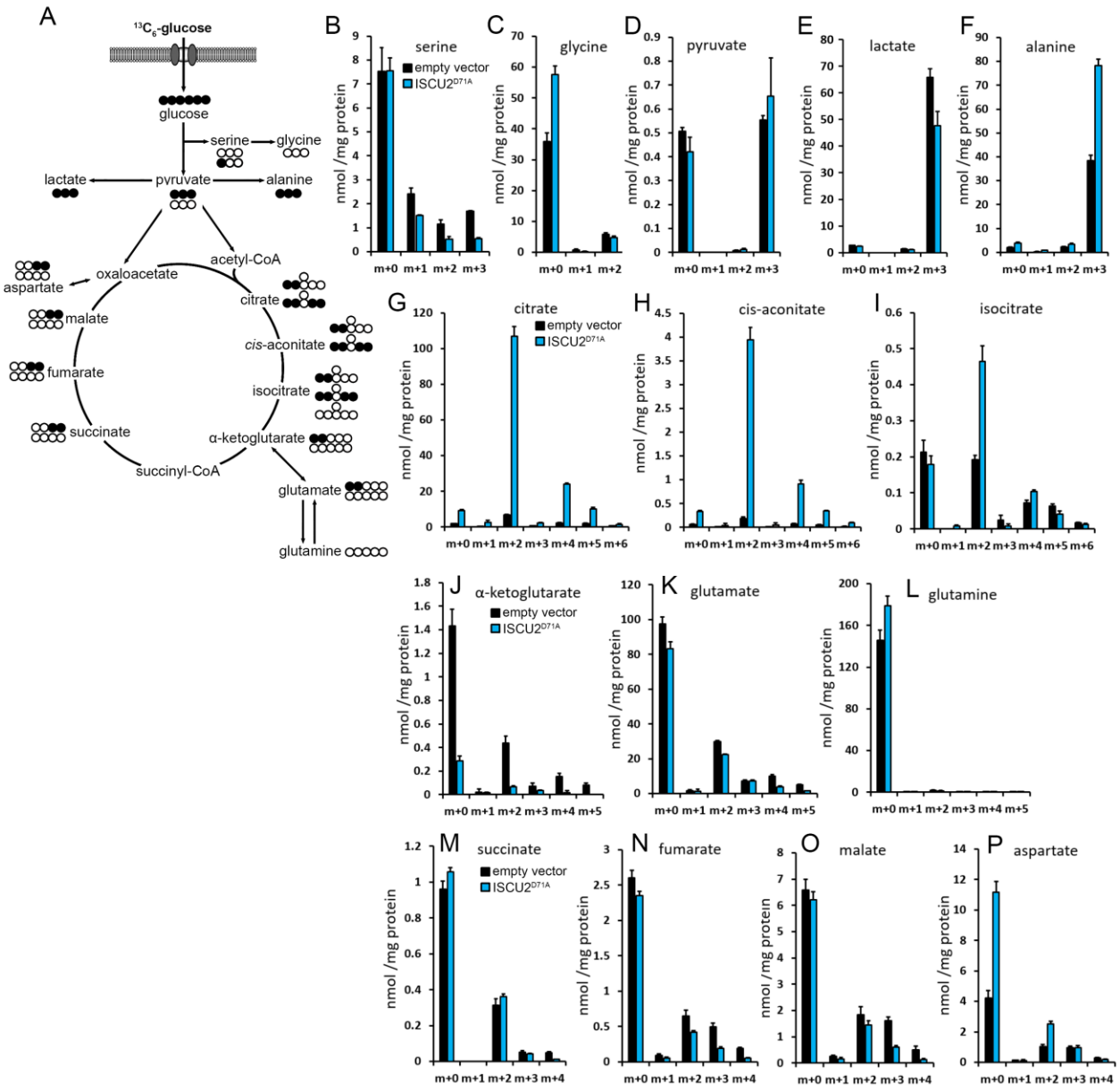


**Figure S2: Fractional isotopologue distribution of selected intracellular metabolites.** (A) Metabolic pathway tracing of TCA cycle and other metabolites in cells expressing ISCU$^{D71A}$. Filled circles represent carbons derived from the $^{13}C_6$-glucose tracer, while unfilled circles represent $^{12}C$ not derived from the tracer. Only isotopologues representing >10% of the total pool of a given metabolite in ISCU$^{D71A}$ cells are shown. (B-P) Total cellular quantities of metabolite isotopologues (n=3, mean±SD). These metabolites were measured by GC-MS, except for pyruvate, lactate and succinate, which were measured by IC-UHR-FTMS. $^{13}C$ enrichment of glycolysis intermediates upstream of pyruvate was essentially 100% (data not shown).

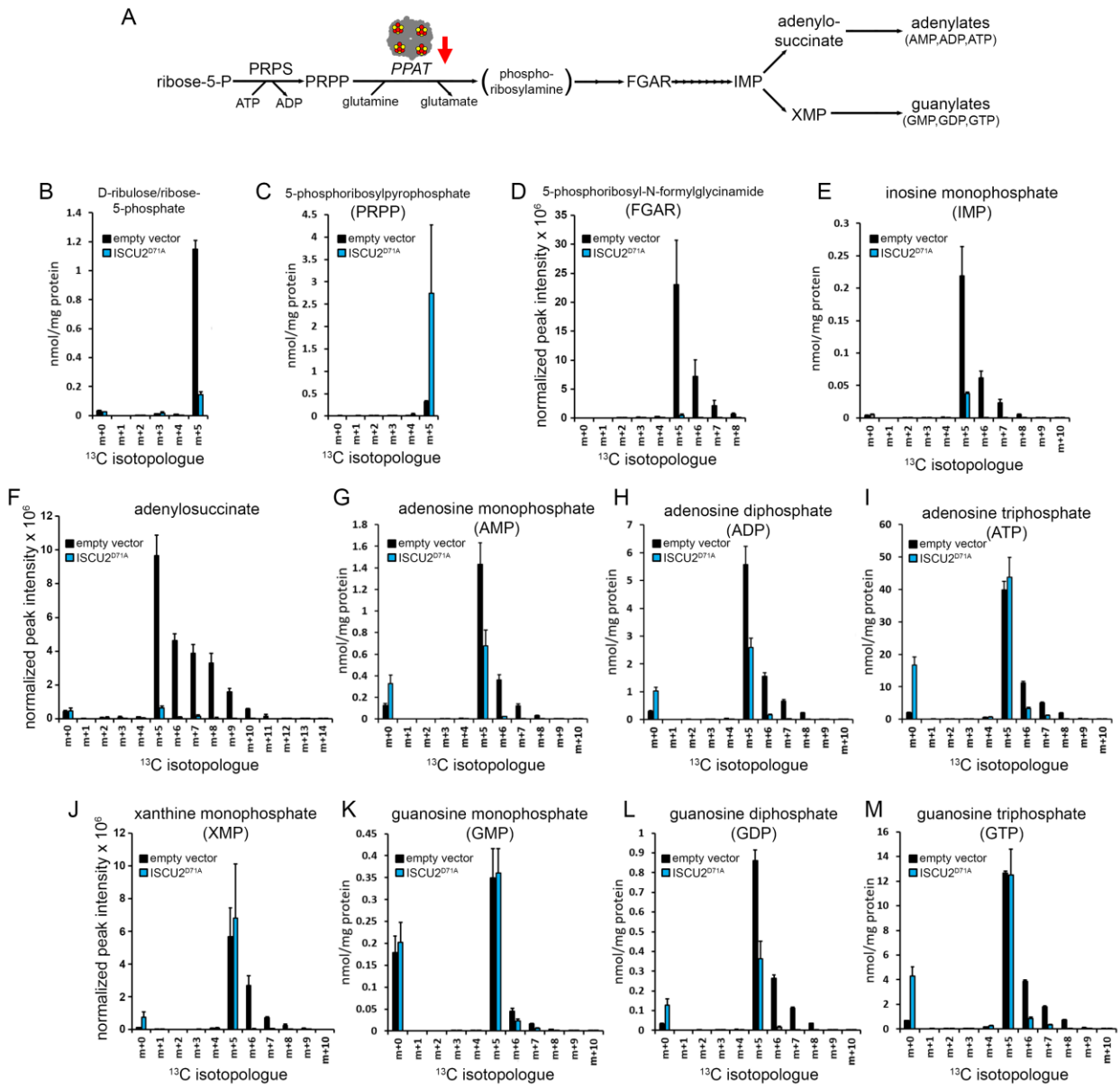


**Figure S3: Analysis of de novo purine biosynthesis.** (A) Schematic diagram outlining *de novo* purine biosynthesis in cells expressing empty vector or ISCU$^{D71A}$. (B-M) IC-UHR-FTMS analysis of $^{13}C$ isotopologue distribution of selected intermediates in the purine biosynthetic pathway. With metabolites for which a standard was not available, data are expressed as normalized peak intensities.

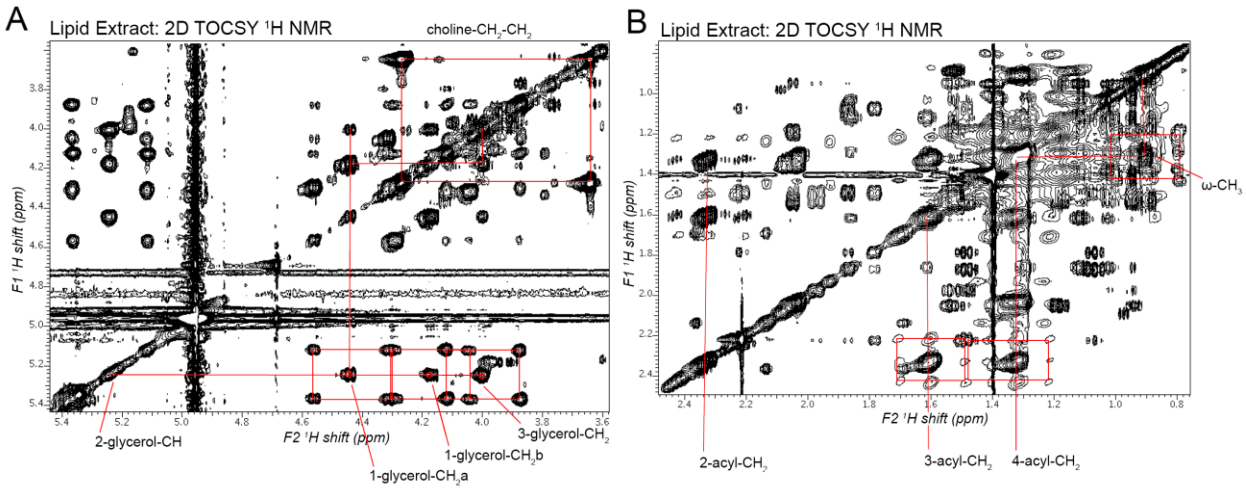


**Figure S4: 2D TOCSY NMR spectra** (A) 2D TOCSY spectrum region showing the glycerol and choline subunits of the glycerophospholipids in HEK293 lipid extracts. As expected, there was no significant $^{13}$C-enrichment in the choline subunits of the glycerophosphocholines, but substantial and equal $^{13}$C enrichment on all three carbons of the glycerol subunits, denoted by the red boxes that connect the $^{13}$C satellite peaks. (B) 2D TOCSY spectrum region showing the fatty acyl chains of the GPLs. The boxes connecting the peaks at 2.3 to 1.6 and 1.32 ppm are the $^{13}$C satellites of the C2-C3 and C2-C4 resonances of the acyl chains respectively. The specific pattern shows that the acetyl-CoA pool comprised a mixture of $^{13}$C 2 acetyl units deriving from $^{13}$C-glucose and from unlabeled sources. The ω-methyl resonances also showed $^{13}$C -2 acetyl units in the acyl chains, indicating that complete chain synthesis had occurred, as these are present only in the complex lipid (e.g. GPL and TAG).

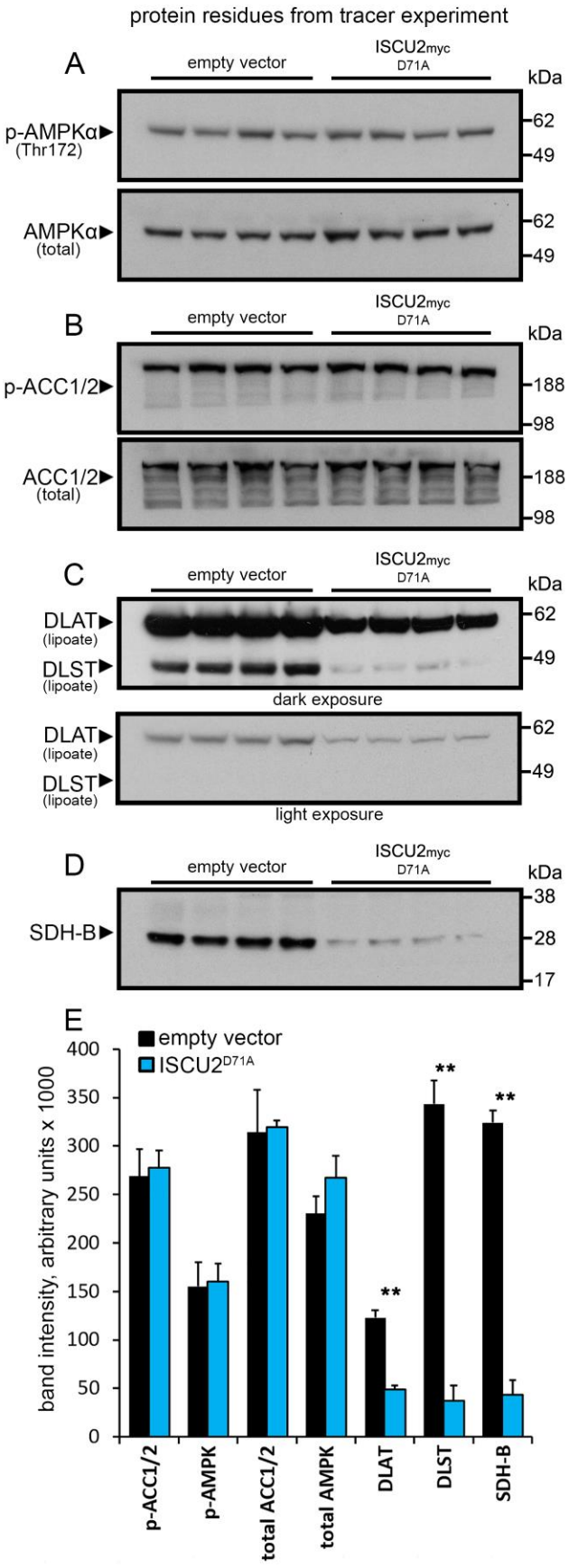


**Figure S5: Immunoblots of proteins obtained from the extracts used for metabolomics experiments.** The protein residues recovered from the Stable Isotope-Resolved Metabolomics (SIRM) tracer experiment presented in Figures 4 and 5 were subjected to SDS-PAGE and immunoblotting. These data indicated (A) no significant change in Thr172 phosphorylation of AMPKα or total AMPKα levels. (B) No significant change in phospho-ACC levels or total ACC levels. (C) A mild decrease in lipoylation of pyruvate dehydrogenase (PDH) subunit DLAT and a strong decrease in α-ketoglutarate dehydrogenase subunit DLST; dark and light exposures of the same immunoblot are shown. (D) Immunoblot for Fe-S-containing subunit SDHB confirmed that this protein was greatly decreased in these samples. (E) Densitometry was applied to the western blots presented in this figure, revealing a significant decrease in DLAT, DLST, and SDH-B protein levels in cells expressing $ISCU2^{D71A}$ protein. (n=4, % control±SD; **p<0.01).

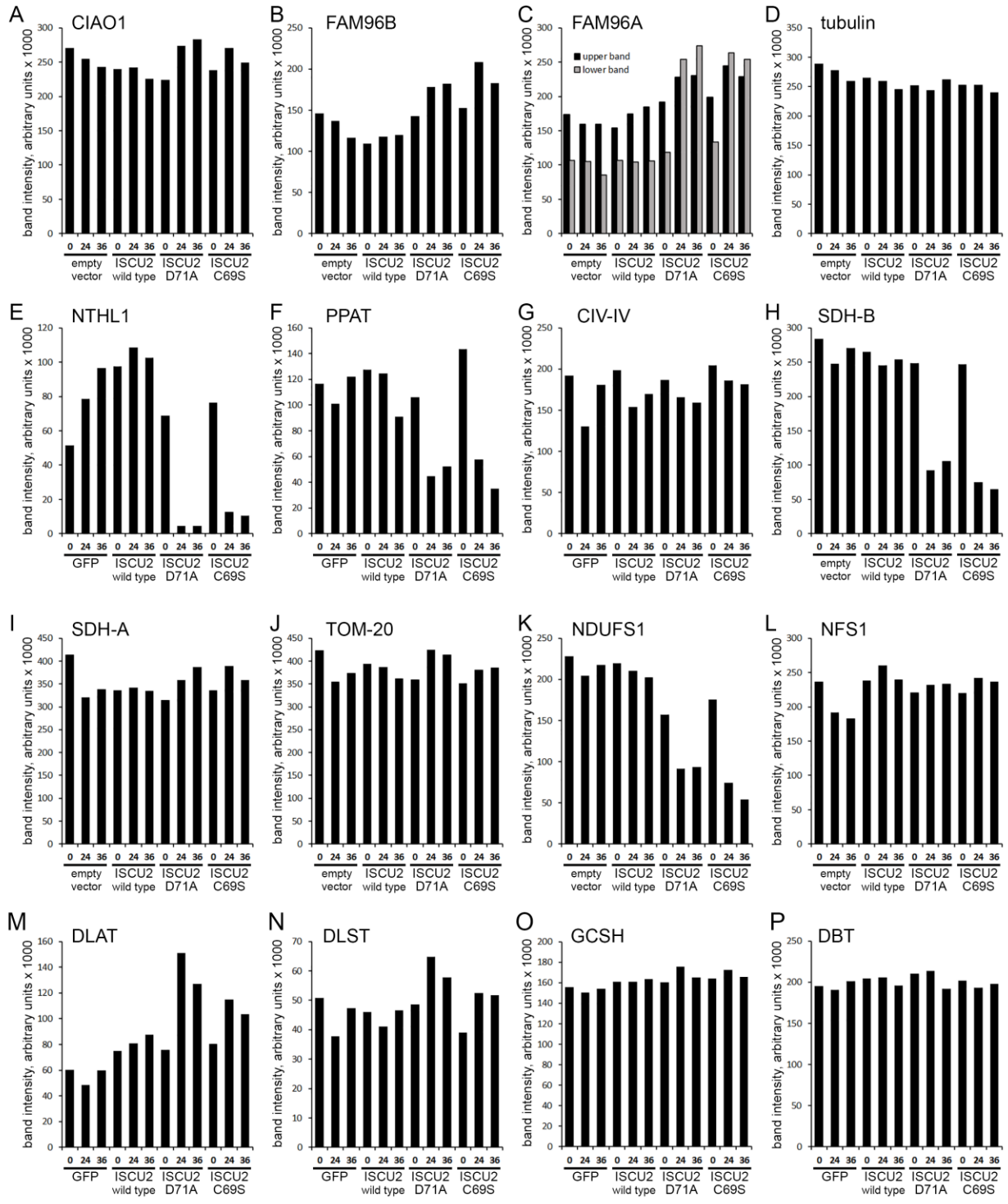


**Figure S6: Densitometry of western blots.** Bands from selected western blots were quantified and normalized to total protein on the membrane as assessed by Ponceau-S staining. (A-D) Quantified bands from Figure 2D. (E-G) Quantified bands from Figure 3A. (H-J) Quantified bands from Figure 3B. (K,L) Quantified bands from Figure 3C. (M-P) Quantified bands from Figure 3F.